Quantum Electronics **38** (5) 409 – 423 (2008)

INVITED PAPER

PACS numbers: 42.55.Px; 42.60.Lh; 42.79.Sz
DOI: 10.1070/QE2008v038n05ABEH013817

Quantum dot diode lasers for optical communication systems

A.E. Zhukov, A.R. Kovsh

***Abstract*. Basic technological and physical aspects of injection lasers based on arrays of self-organised InAs/InGaAs quantum dots on GaAs substrates for optical communication systems in the 1.2 – 1.3 μm spectral range are considered. The possibility of simultaneous lasing at a great nimber of longitudinal modes at a high power level and low noise is demonstrated. The use of these lasers in wavelength-division-multiplexing systems based on the spectral separation of the laser output spectrum is substantiated.**

Keywords: *quantum dots, quantum wells, gain, emission spectrum, optical communication.*

1. Introduction

Optical communications require a laser emitting at a wavelength for which the optical loss in a medium of propagation is minimal. For this reason, laser diodes emitting at wavelengths within the C band (1530 – 1565 nm) attract the main attention. Due to a low optical loss (about 0.2 dB km^{-1}) in standard optical fibers, this spectral band is used in the long-haul optical communication systems. At the same time, the O band ($\sim$1.26 – 1.36 μm) seems to be attractive for optical communications over intermediate distances (several tens of kilometers or shorter). Optical data transmission at the wavelength where the chromatic dispersion is close to zero (1310 nm for a standard single-mode silica fiber) can be performed with a higher bit rate. For optical communication over ultra-short ranges (e.g., within an optoelectronic chip) it is attractive to use SiGe waveguides buried in a silicon substrate under silicon-based integrated circuits. Such waveguides containing approximately 2 % – 5 % of germanium are transparent for optical radiation with wavelengths longer than 1.2 μm (fabrication method of planar SiGe waveguides in a silicon matrix is described, e.g., in Ref. [1]). Their use in data processors may lead to a significant increase in the clock rate due to elimination of the problem of electrical data transmission over wires. All these provoke interest in the development of diode lasers emitting in the 1.2 – 1.3 μm range.

The well developed technology of diode lasers emitting in the 1.55-μm region is based on either InGaAsP or InGaAlAs semiconductor heterostructures grown on InP substrates. Over a long period of time the same materials have been also considered as the only candidates for laser sources operating at shorter wavelengths. However, it was found that shorter-wavelength lasers made of these materials suffer from poor temperature stability caused by reduced band-edge discontinuities at heterointerfaces. For instance, in the case of 1.3-μm InP lasers the energy gap between the quantum-well (QW) optical transition energy and the bandgap of cladding layers is only 0.4 – 0.45 eV, while the characteristic temperature of the threshold current is ususally 60 K for InGaAsP/InP [2] and 90 – 110 K for InGaAlAs/InP [3]. At the same time, 0.98-μm lasers on GaAs substrates for which the overall band-edge discontinuity is about 0.55 eV, have considerably higher typical values of T_0 ($\sim$150 K), whereas the record value of T_0 exceeds 300 K [4].

Heterostructures grown on GaAs substrates eliminate the problem of thermal escape of charge carriers [5] due to the possibility of employing AlGaAs or In(Al)GaP wide-bandgap emitter layers. The main difficulty in the design of diode lasers on GaAs substrates emitting in the 1.2 – 1.3-μm spectral range is associated with the lack of semiconductor compounds having suitable bandgap and being lattice-matched to the GaAs substrate. Strained QWs are incapable of providing a wavelength noticeably exceeding 1.2 μm due to limitations imposed on the indium composition and their thickness by the border of dislocation-free growth [6]. At the same time, it was found that self-organised InAs quantum dots (QDs) are very promising for obtaining lasing in this spectral range. This approach gives a chance to combine possibility of reaching the required wavelengths in diode lasers grown on GaAs substrates with all advantages expected for a laser based on an active region with zero-dimensional size quantisation [7]. In particular, quantum dot lasers can provide simultaneous emission at a large number of longitudinal modes possessing a high power level and a low noise. Such lasers may find application in wavelength-division-multiplexing (WDM) optical communication systems avoiding many obstacles inherent in conventional single-frequency laser diodes.

A.E. Zhukov St. Petersburg Physics and Technology Centre for Research and Education, Russian Academy of Sciences, ul. Khlopina 8/3, 194021 St. Petersburg, Russia; e-mail: zhukov@beam.ioffe.ru;
A.R. Kovsh Innolume GmbH, Konrad-Adenauer-Allee 11, 44263 Dortmund, Germany

Received 22 December 2007
Kvantovaya Elektronika **38** (5) 409 – 423 (2008)
Translated by A.E. Zhukov

2. Formation of self-organised quantum dots

The density of states in a two-dimensional quantum well represents a step of height $m/(\pi\hbar^2)$ (m is the effective mass) beginning from the quantum subband energy. Therefore, charge carriers may populate the states in a broad energy interval above the subband edge. The transparency current density (i.e. a current density required for achieving the population inversion in the active region) is specified by a product of the height of the density of states and the thermal broadening of the Fermi function, thus giving approximately 50 A cm^{-2} at room temperature. Because the density of states is virtually independent of quantum well structural parameters, it is impossibly to built a quantum well that provides a noticeably lower density of the transparency current.

At the same time, the density of states of a QD array is determined by the array surface density n_{QD}, which can be, in general, infinitely low. For example, in the case of an absolutely uniform QD array, the density of states can be represented by the delta-function, $2n_{QD}\delta(E - E_{QD})$, centered at a quantum level E_{QD}. Hence, taking a proper choice of the surface density of quantum dots, one can achieve a lower transparency current density compared to that of a two-dimensional quantum well. For instance, the array surface density n_{QD} of the order of $\sim 10^{10}$ cm^{-2} may provide a transparency current density of about 5 A cm^{-2}. Another important advantage of a laser based on an ideal array of QDs is the temperature independence of its threshold current which is a result of a narrow width (as compared to the thermal energy) of the density of states.

The search for a method suitable for the formation of uniform arrays of defect-free semiconductor objects of sufficiently small dimensions was one of the main directions in the development of the technology of semiconductor material synthesis in the late 1980s and early 1990s. The self-organisation of strained islands, also called the Stranski–Krastanow growth mechanism, which was first observed in 1984 [8], is currently the most successful practical technology for formation of nearly ideal quantum dots. An array of self-organised quantum dots is formed upon epitaxial deposition of a thin InAs layer on a GaAs substrate. Lattice mismatch in this material system is about 7%. The possibility of partial relaxation of elastic strain in apical zones of three-dimensional islands is just the driving force for formation of the quantum dot array upon reaching a critical layer thickness of 1.7 monolayers ($\sim$0.5 nm). Depending on deposition conditions and the amount of deposited InAs, QDs are usually 8–15 nm in base and about 3–5 nm in height; the array density is approximately $(3-5)\times 10^{10}$ cm^{-2} (Fig. 1).

InAs QDs remain elastically strained (dislocation-free) in a narrow interval of effective thicknesses from 1.7 to 3–3.5 monolayers, so that precise monitoring of the amount of deposited material is extremely important. In this respect, molecular beam epitaxy is a convenient method of their synthesis due to low growth rates (the deposition rate of InAs is typically about 0.025 nm s^{-1}), fast switching of fluxes, and the possibility of visual monitoring of QD formation by observing changes in the diffraction pattern of high-energy electrons reflected from the growth surface. The high purity of both load materials and a residual atmosphere in a vacuum chamber is exceedingly important for obtaining intense QD luminescence because QDs are typically deposited at low temperatures (around 480 °C) in order to avoid reevaporation and intermixing of the deposited material.

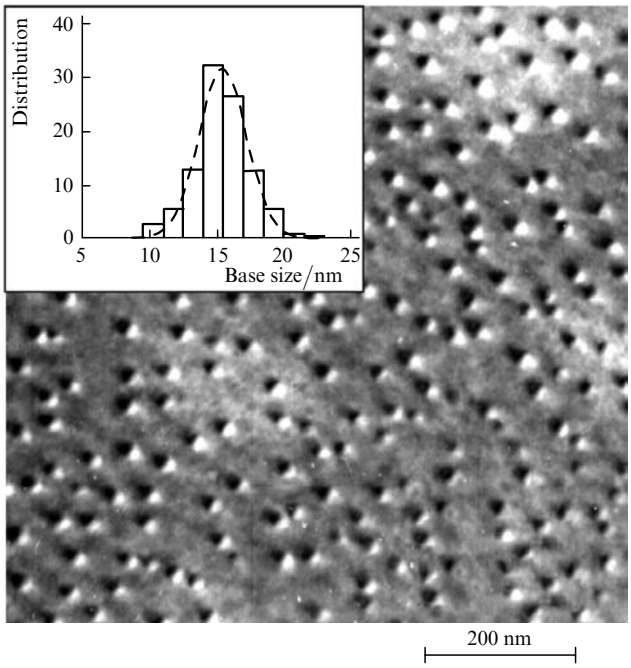

Figure 1. Plan-view bright-field transmission electron microscopy image ($g = 220$ diffraction condition) of a structure comprising quantum dots formed by deposition of 3.5 monolayers of InAs in a GaAs matrix. The surface density of the array is $(3.7 \pm 0.4)\times 10^{10}$ cm^{-2}. Insert shows a histogram of base size distribution to be 15.4 ± 2.1 nm.

The emission wavelength of InAs quantum dots in a GaAs matrix can be controlled by varying the effective thickness Q_{QD} of deposited InAs layer (Fig. 2a), and other deposition conditions (e.g., the growth temperature). A larger effective height of QDs as compared to a two-dimensional quantum well enables achieving emission at $\sim$1.2 μm at room temperature [9]. Further increase in the wavelength is limited by a decrease in the luminescent intensity from islands of a larger size caused by plastic strain relaxation.

Emission at longer wavelengths was achieved by forming quantum dots of a larger size by the method of atomic layer epitaxy (ALE), i.e. the alternating deposition of elements [10, 11]. However, QDs formed by the ALE method and emitting around 1.3 μm are characterised by a low surface density [12], which is 3–5 times lower than typical values for self-organised QDs on GaAs formed under the standard regimes of epitaxial growth. This drawback can be avoided by placing an array of quantum dots in a narrow-bandgap (as compared to GaAs) matrix [13]. For example, regrowth of an array of InAs QDs with an $In_xGa_{1-x}As$ layer ($x \sim 10\%-20\%$) having a thickness of 4–12 nm allows shifting the emission maximum within the 1.1–1.34 μm interval. The emission wavelength of such InAs/InGaAs quantum dots is controlled by three parameters: the effective thickness of InAs spent for island formation (Q_{QD}), the quantum well width (L_{QW}), and the indium content in the quantum well (x_{QW}). The latter two parameters jointly determine the effective bandgap of the quantum well. As an example, Fig. 2a depicts the photoluminescence peak position of InAs QDs covered with a $\sim$5-nm thick

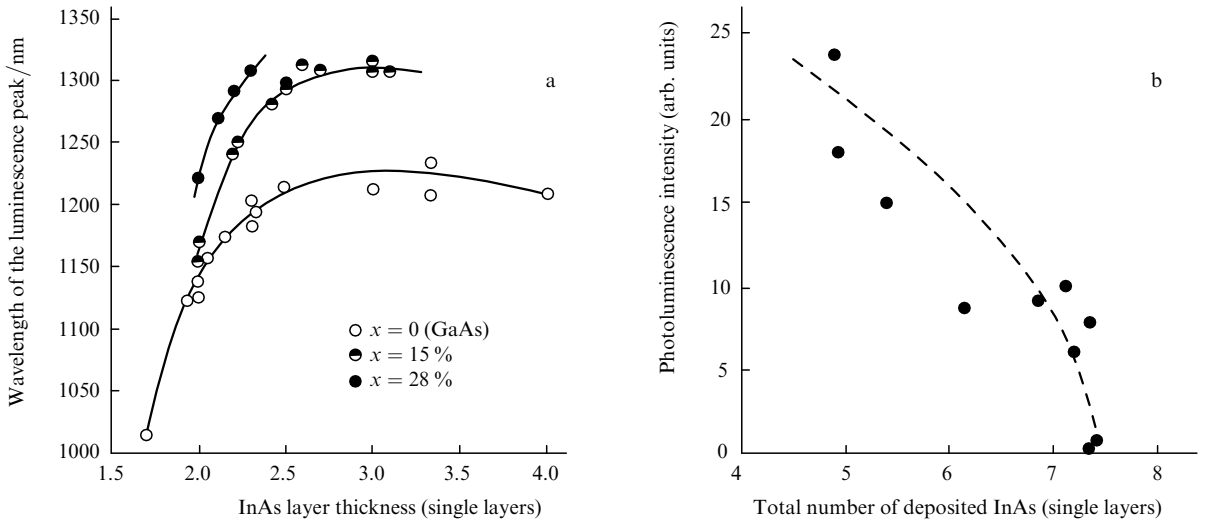

Figure 2. Photoluminescence peak position for QDs covered with layers of $In_xGa_{1-x}As$ of different chemical composition as a function of thickness of deposited InAs (a); dependence of photoluminescence intensity on the total amount of indium for QDs with emission wavelength of $\sim$1.3 μm (b).

$In_xGa_{1-x}As$ layer having the indium content (x) of either 15 % or 28 %. One can see that as the bandgap of the matrix surrounding the quantum dots decreases, the luminescent maximum shifts to the red. Note that in addition to the bandgap of the matrix, the emission wavelength of the quantum dots is also affected by certain modifications in their shape, size and strain which occur upon their re-growth with the InGaAs layer [14].

An advantage of the method of controlling the quantum dot wavelength by varying the matrix chemical composition is that the quantum dot array itself can be formed under conditions most optimal for its uniformity, luminescence intensity, etc. For example, a similar wavelength can be obtained by using different sets of parameters Q_{QD}, L_{QW}, and x_{QW}. However, a luminescence intensity and a laser threshold current density are quite different for various sets of the parameters. It was found that the brightest luminescence among different structures of a specified wavelength is achieved if an overall quantity of deposited InAs (i.e., $Q_\Sigma = Q_{QD} + L_{QW}x_{QW}$) is minimised (Fig. 2b) because such minimisation reduces the total mechanical strain and, consequently, the probability of dislocation formation.

3. Threshold current density and optical gain in a QD laser

Lasing in a structure with self-organised quantum dots was demonstrated for the first time in 1994 [15] at liquid nitrogen temperature. Further studies of stripe laser diodes [16] have revealed optical gain saturation and thermally activated escape of charge carriers into upper energy states, which was manifested in a steep increase in the threshold current density and a blue shift of the lasing wavelength with increasing the optical loss and/or temperature. Due to a limitation imposed on the density of states of a QD array by its surface density, the optical gain acquires a finite value called the saturated gain G_{sat}. The scatter in island sizes leads to the inhomogeneous broadening of the optical transition and proportional decrease in G_{sat}. Experimental values of the saturated gain at the ground-state optical transition in long-wavelength InAs/InGaAs QD lasers range from 3 to 6 cm^{-1} per QD layer [17–19] depending on QD formation regimes and the design of a laser waveguide. A high localisation energy leads to the appearance, in addition to the ground-state optical transition GS, of several excited-state optical transitions separated from each other by a nearly equal energy interval of about 70 meV (Fig. 3a). If optical losses in a laser resonator exceed the saturated gain at the ground-state optical transition, lasing proceeds at a shorter wavelength of the excited-state optical transition characterised by a higher saturated gain (Fig. 3,b).

Because lasing at the longest wavelength (at the ground-state optical transition) is of the most practical interest, several methods have been proposed for increasing the saturated gain in a QD laser, including formation of denser or more ordered QD arrays. However, the use of several QD layers in the laser active region providing the increase in the saturated gain by several times, proved to be the most practicable. The dependences of the threshold current density on the number of QD layers calculated on the basis of up-to-date information on the transparency current density and the saturated gain per one QD layer are presented in Fig. 4a for different total optical losses α. The presence of a minimum in these dependences is explained by the fact that both the saturated gain and the overall transparency current density are proportionally scaled with the number of QD layers [17]. One can see that for G_{sat} of about 20–30 cm^{-1}, as it is usual in stripe lasers, the optimum number of the layers corresponds to approximately 10.

The successive deposition of several QD layers is possible if the layers are separated by so-called spacers of an unstrained material [20], as is illustrated in Fig. 4b. The use of multilayer arrays emitting at 1 μm resulted in the reduction of a room-temperature threshold current density down to $\sim$100 A cm^{-2} and led to the first realisation of cw lasing [21].

Lasing at 1.3-μm was demonstrated for the first time in 1998 in a structure based on quantum dots formed by the ALE method [22]. However, a low surface density of such QDs, which significantly restricts their optical gain, has forced to focus efforts on the development of diode lasers based on InAs QDs placed in an InGaAs quantum well.

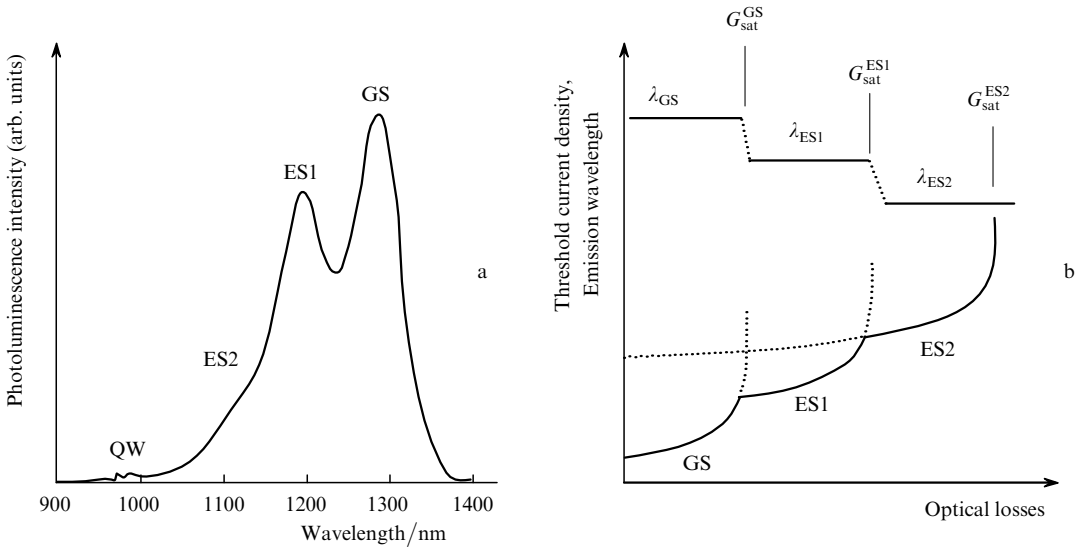

Figure 3. Photoluminescence spectrum of an InAs/InGaAs array with several excited-state optical transitions (a); schematic dependences of the threshold current density and the lasing wavelength on optical losses taking into account the ground-state and excited-state optical transitions (b).

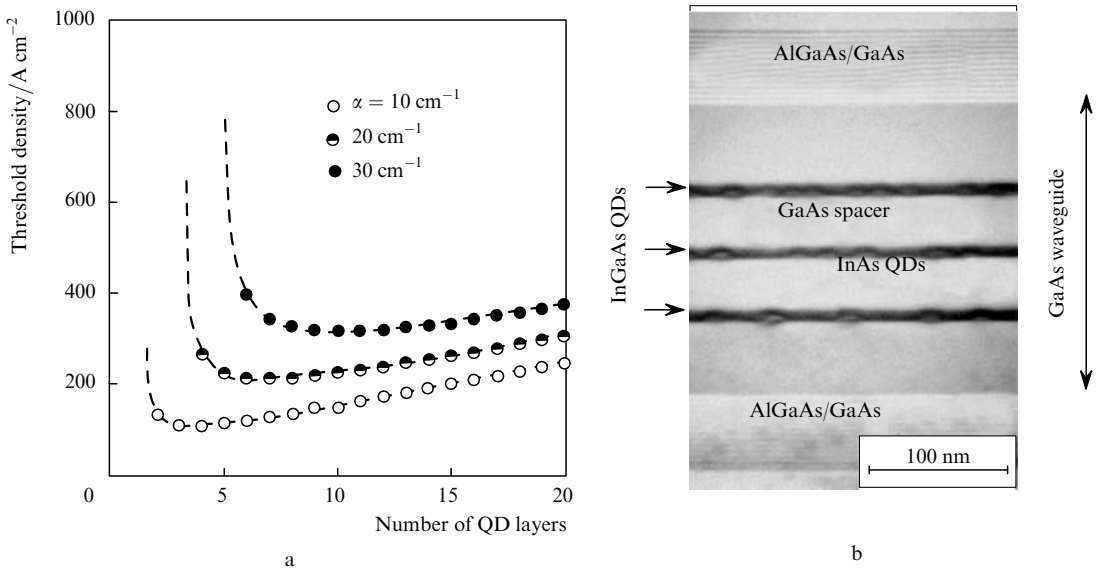

Figure 4. Calculated dependence of the threshold current density for the ground-state lasing ($\lambda \sim 1.3$ μm) on number of quantum dot layers at different levels of optical losses in a laser cavity (a); cross-section transmission electron microscopy image for a laser structure comprising three layers of InAs/InGaAs QDs.

Room-temperature lasing in InAs/InGaAs QDs was achieved in 1999 [23, 24]. Shortly thereafter continuous wave operation has been attained [25]. However the earliest lasers of this kind emitted at 1.24–1.25 μm. Attempts to reach longer wavelength led to a noticeable increase in the threshold current density (Fig. 5a) due to formation of defects in the highly strained active region. Since then the wavelengths of low-threshold lasing has been extended to 1.33 μm due to the aforementioned optimisation of multilayer QD arrays and the strain minimisation in each QD layer.

Quantum dots emitting at longer wavelengths and, consequently, containing larger volumes of a strained material require thicker spacers. In addition, an increase in the spacer thickness leads to a decrease in the optical confinement factor of outer QD layers situated far from the waveguide center. It is currently assumed that the spacer thickness of 30–35 nm is optimal for structures with 10 QD layers. Figure 5a shows the dependence of the optical gain and the lasing wavelength on the pump current for a laser having the active region of this kind [26]. One can see that the highest optical gain is 45–46 cm^{-1}, while the lasing wavelength may exceed 1.32 μm.

A high optical gain of the laser active region makes it possible to use laser cavities with a high mirror loss. It is also favourable that the internal loss of properly designed QD lasers decreases with increasing the saturated gain [27] and with increasing the localisation energy [28]. The experimental dependence of the internal loss on the number of QD layers in 1.3-μm lasers is shown in Fig. 6. One can see that the internal loss of a 10-stacked QD laser is as low as 1.2 cm^{-1}. In combination with the internal differential

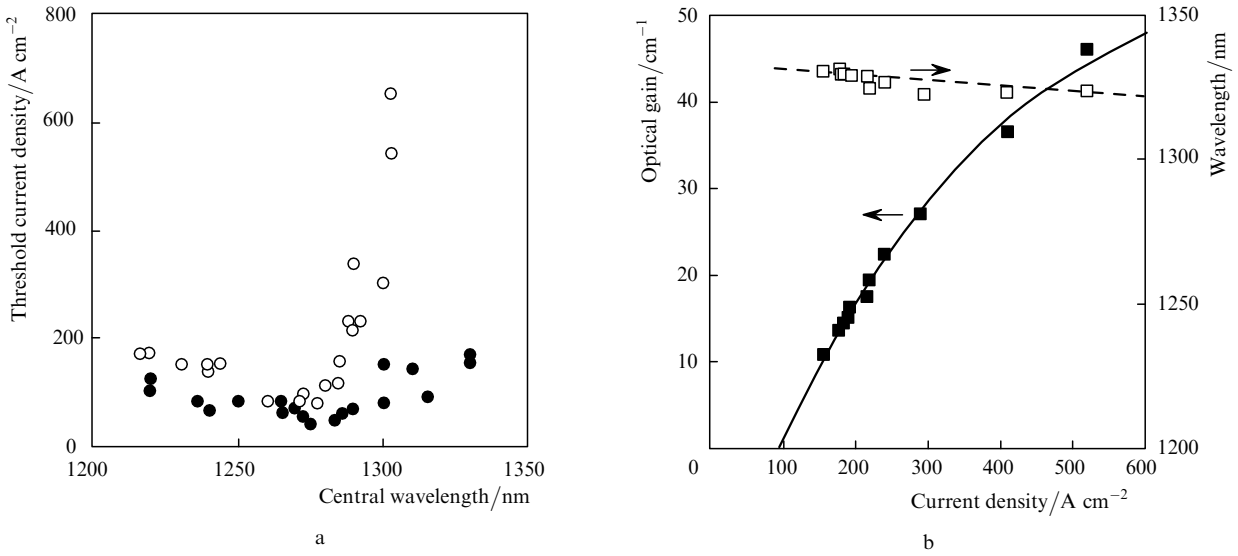

Figure 5. Dependence of the minimum threshold current density on lasing wavelength for various lasers based on InAs/InGaAs QDs: initial experiments (open circles) and results of optimisation (solid circles) (a); dependence of the optical gain and the lasing wavelength on the pump current for a laser based on 10 layers of QDs (b).

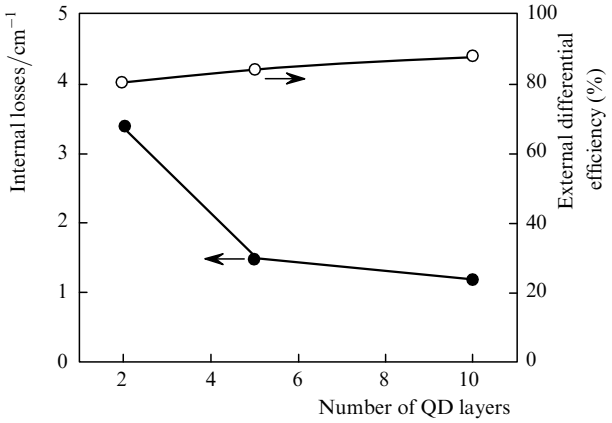

Figure 6. Dependence of the internal loss (solid circles) and the maximum external differential efficiency (open circles) on the number of QD layers in an active region of lasers emitting at ~1.28 μm.

efficiency in excess of 90 %, this results in a high external differential efficiency (the highest reported value is 88 % [29]) (Fig. 6).

When the mirror loss is low because of long resonator lengths and/or highly reflecting mirrors, the use of long-wavelength QD arrays in the laser active region may reach an extremely low threshold current density. For example, the threshold current density as low as 24 and 25 A cm^{-2} has been reported for lasers with resonator lengths of 19.2 and 14.2 mm, respectively, emitting at 1.285 and 1.32 μm [30, 31]. The record-low threshold current density of 19 A cm^{-2} has been achieved in a 1.33-μm stripe laser with an oxide-confined aperture and high reflective facet coatings (the external differential efficiency was only 2 %) [32]. These figures are the lowest values for any sort of stripe lasers operating at room temperature. The previous best value that belongs to quantum well lasers was about ~50 A cm^{-2} [33, 34]. Let us emphasise that the threshold current density reduction in lasers operating in the low-loss regime is achieved not only due to a low density of electron states in the QD array but also because of longer emission wavelength of those lasers which implies deep localisation of the ground state level with respect to the surrounding matrix.

The use of few millimeter long resonators is especially important in the case of mode-locked lasers because a pulse repetition rate is inversely proportional to a laser length. For example, a 5-GHz repetition rate (Fig. 7,a) needs a resonator length of about 8 mm. Capability of achieving sufficiently intense and short optical pulses with repetition rates of 5 – 10 GHz opens up the way for applications of mode-locked diode lasers as clock generators in integrated circuits with optical data transmission [35]. QD lasers are excellent candidates for such applications, because their low internal loss is favourable for achieving an acceptably high differential efficiency even in long laser diodes, while a low density of states permits readily bleaching a QD passive section.

A passively mode-locked QD laser was demonstrated for the first time in 2001 ($F = 7.4$ GHz) [36]; hybrid mode-locking regime was reported in 2003 ($F = 10$ GHz) [37]. The highest up-to-date pulse power of 1.7 W in a fully monolithic diode laser was demonstrated in Ref. [38]. Figure 7b displays the dependence of the pulse power and the pulse width on an average laser power. Though the average power increases with increasing the current through a gain section, higher currents lead to broadening of the optical pulses. These two trends oppositely affecting the pulse power jointly determine an optimum operating point of a mode-locked laser diode. Pulses of the highest power are achieved at a moderate average power when the pulses have the shortest width. The mode-locking regime of laser operation is also suitable for generation of optical pulses with a repetition rate beyond the limiting cutoff frequency of direct modulation. For example, a 50-GHz repetition rate has been demonstrated for QD lasers [39].

It should be noted that the direct modulation frequency in state-of-the-art 1.3 μm QD lasers has been estimated to be 7 – 8 GHz; data transmission with a 10 Gb s^{-1} bit rate has been demonstrated [40, 41]. Unlike QW lasers, where direct modulation is limited by a relaxation oscillation frequency,

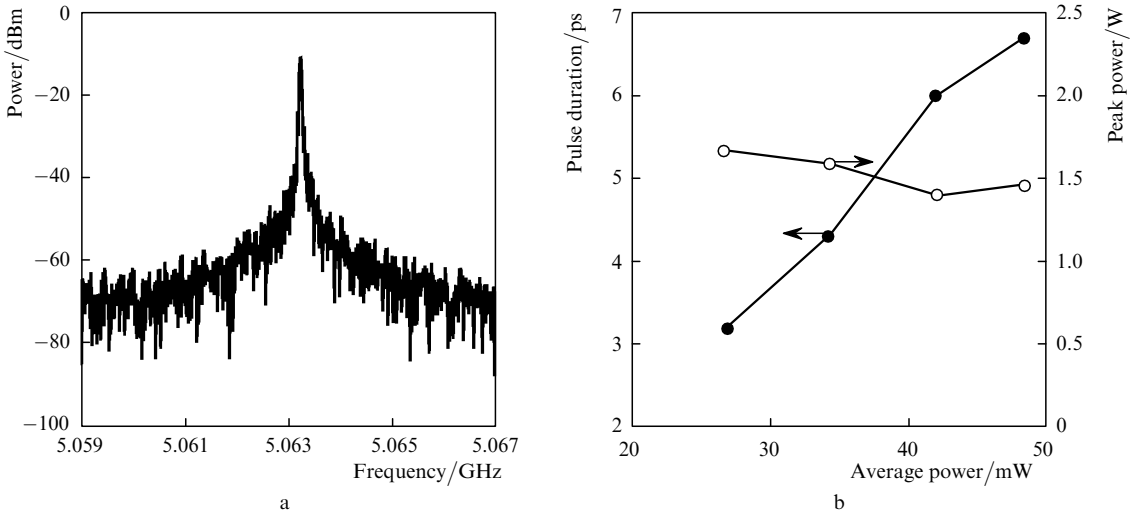

Figure 7. Frequency spectrum (a) and dependences of the pulse width (solid circles) and the pulse power (open circles) on average power (b) for passively mode-locked QD lasers.

the relaxation oscillations are strongly damped in QD lasers and the modulation frequency is limited by the *K*-factor. Despite relatively low maximal modulation frequency, QD lasers have a significant advantage over QW counterparts, which consists in high temperature stability of their characteristics. In particular, a 10-Gb s^{-1} direct modulation has been demonstrated in Ref. [41] with a fixed (without any temperature compensation) modulation current and a fixed bias current in the temperature interval of 20 – 90 °C.

The independence of the threshold current of QD lasers on temperature was predicted in [7]. According to the prediction, already the earliest lasers based on self-organised QDs demonstrated a nearly infinite characteristic temperature [42] at low environment temperatures (below ~200 K) or even a negative characteristic temperature [43], i.e. temperature-induced decrease in the lasing threshold. However, till recently the experimental results for operation at room temperatures have revealed relatively low characteristic temperatures ($T_0 \sim 50 - 60$ K). It was found that a high temperature stability of the threshold current is followed by its drastic increase with increasing temperature, so that $J_{th}(T)$ dependence has a characteristic break. Figure 8a illustrates the fact that an interval of high T_0 extends towards higher temperatures when a localisation energy of the ground-state QD level increases (i.e., the lasing wavelength increases) or when the saturated gain (i.e., the number of QD layers) increases [24]. Such a behavior indicates that the threshold current density of a QD laser may be significantly affected, at least at elevated temperatures, by recombination (in particular, nonradiative recombination) of charge carriers that populate the matrix states. Progress in the technology of multilayer long-wavelengths QDs led to a considerable increase in T_0 in QD lasers (up to 150 K for 80 – 90 °C [44]).

By applying the modulation doping technique [45], the temperature stability of the threshold current has been

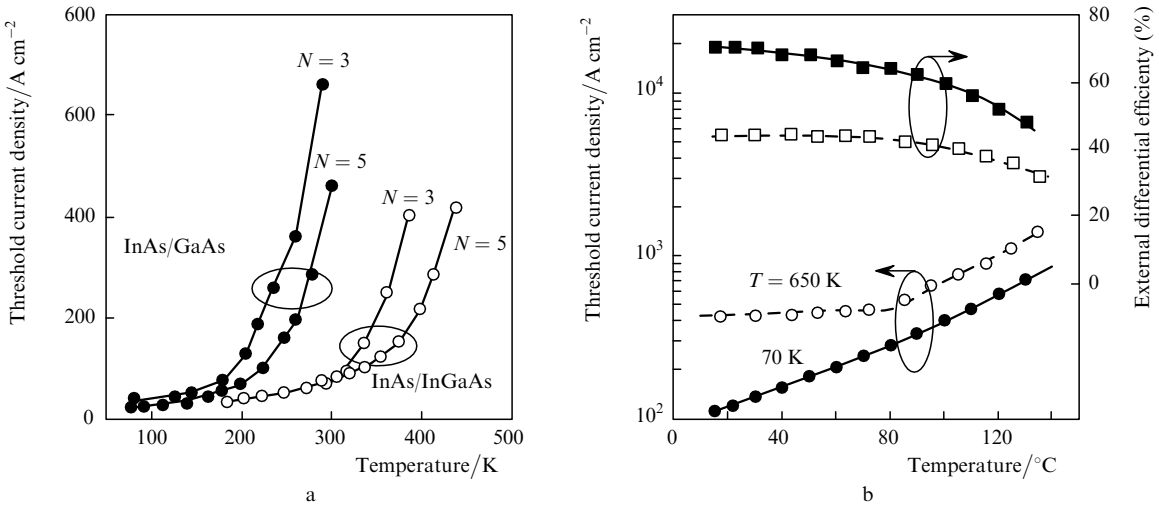

Figure 8. Temperature dependence of the threshold current density for lasers with the various number *N* of QD layers and different design of the active region: solid circles – InAs QDs in a GaAs matrix ($\lambda \sim 1.05$ μm); open circles – InAs QDs in an InGaAs quantum well ($\lambda \sim 1.27$ μm) (a); temperature dependences of the threshold current density (circles) and the external differential efficiency (squares) for an undoped structure (solid symbols) and for a structure with a p-doping level of 2×10^{12} cm^{-2} per QD layer (open symbols) (b).

considerably improved. The method consists in adding acceptor-type dopants into spacer layers between QD layers to reach a p-doping level of several tens of holes per one quantum dot in the active region. It was mentioned that the improved temperature stability may be associated with reduced thermal population of closely spaced hole subband levels [45] as well as suppression of the rate of Auger recombination [46]. Already initial experiments have demonstrated a characteristic temperature in excess of 200 K over the temperature interval of $0-80\,^{\circ}\mathrm{C}$ [47]. Further optimisation has led to complete temperature independence of the threshold current ($T = \infty$ up to $75\,^{\circ}\mathrm{C}$ [46]). Figure 8b illustrates how a temperature dependence of a threshold current density of QD lasers is changed with increasing a p-type doping level. Note, however, that the increase in T_0 with increasing the dopant concentration is accompanied by the increase in the absolute value of the threshold current density and the decrease in the external differential efficiency caused by a rise of the internal loss.

For a long period of time a reliability of long-wavelength QD lasers gave rise to doubts because of a severe strain in the active region. Accelerated aging tests have been carried out for 1.3-μm QD lasers operating at different temperatures (65 and $85\,^{\circ}\mathrm{C}$) for 2070 hours at a fixed drive current of 350 mA (Fig. 9) [48]. During the accelerated aging test none of 15 lasers reached the failure criteria (20-% decrement of an initial output power). A median time-to-failure was evaluated by extrapolating the experimental data to be 1.4×10^5 and 3.2×10^3 hours for lasers operating at 65 and $85\,^{\circ}\mathrm{C}$, respectively. An average lifetime of a normal operation condition ($40\,^{\circ}\mathrm{C}$) was estimated from a temperature dependence of the median time-to-failure to be 1.2×10^6 hours.

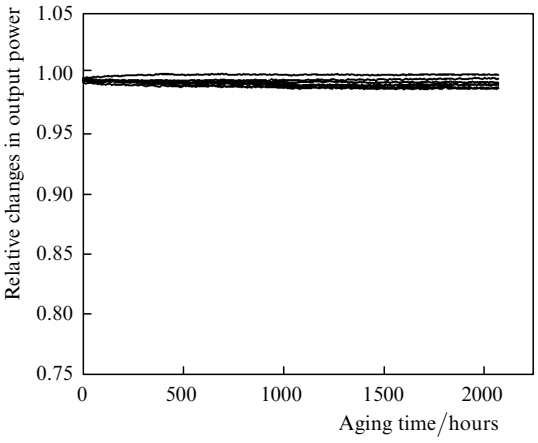

Figure 9. Normalised output power of a group of QD lasers as a function of aging time for a cw operation at $65\,^{\circ}\mathrm{C}$.

4. Formation of broad gain and lasing spectra

Lasing in a Fabry–Perot cavity arises at a longitudinal mode whose wavelength is the closest to a maximum of the gain spectrum of an active region. However if no special measures are undertaken to ensure single-frequency lasing, an increase in the pump current beyond a lasing threshold leads to excitation of additional side modes. As a result, the emission spectrum of the laser broadens. Multifrequency lasing is caused by a relatively small (as compared to a width of the gain spectrum) spectral separation between neighboring longitudinal modes and inhomogeneous gain saturation. This phenomenon, also known as spectral hole burning, consists in the decrease in the optical gain at a lasing wavelength with increasing a number of photons in the laser cavity. In brief, an empty electronic state arisen from a stimulated emission event has to be populated by a charge carrier before a next phonon emission event may take place. A finite rate of the population of an electronic state may lead to a decrease in the number of charge carriers capable of maintaining the laser action, which reduces the gain at the given wavelength and facilitates excitation of side modes.

The width of a multimode lasing spectrum may not exceed the width of the gain spectrum. To obtain a broad gain spectrum, it is more preferable to use an array of self-organised QDs as the active region compared to QWs. If the population of the upper states can be neglected, the QD ground state is completely populated when a pumping level reaches a double transparency current density. The gain spectrum simultaneously reaches a width of inhomogeneous broadening of the optical transition, which can be as large as several tens of nanometers. Because the transparency current density is determined only by the surface density of the QD array and independent of the inhomogeneous broadening, it is possible to vary the gain spectrum width and the corresponding level of pumping irrespective of each other. Moreover, low surface densities of QD arrays enable achieving significant widths of the gain spectrum even at relatively low currents.

For noticeable manifestation of the inhomogeneous gain saturation effect, the rate of population of the electronic states in the active region should be suppressed to a great extent. In a QD laser, unlike a QW laser, the electronic states of different energies belong to different spatially separated QDs in the array. Therefore, the population of electronic states in a QD laser may be significantly suppressed [49] and, consequently, the broadening of the laser spectrum can be much greater than in a QW laser. For instance, the population time of the empty ground state of QDs emitting at 1.3 μm was estimated to be 2.5 ps [50].

The emission spectra of a QD laser of width of $\sim 50-60$ meV at 80 K were presented in Ref. [51]. The room-temperature spectra of QD lasers of width $\sim 8-15$ nm were demonstrated in [52–54]. However, either the spectral power density or the spectral bandwidth was insufficient for a practical application of such lasers. We demonstrated for the first time that it is possible to achieve simultaneously a spectral bandwidth in excess of 15 nm and a spectral power density of more than 10 mW nm^{-1} [55] in a diode laser based on self-organised QDs. This combination of parameters in conjunction with a central wavelength at ~ 1.3 μm makes such lasers promising for applications in multichannel optical communication systems.

If nearly all QDs of an array (N_{QD}) are involved in lasing, the laser linewidth Δ_{las} will approximately coincide with the inhomogeneous width Δ of the ground-state optical transition. If a smaller number N_{las} of QDs contributes to lasing, the laser linewidth decreases accordingly to $\Delta_{\mathrm{las}} \approx (N_{\mathrm{las}}/N_{\mathrm{QD}})\Delta$. The number N_{las} can be evaluated as a ratio of a pump current I to a maximum recombination current that can flow through a single QD ($2e/\tau_{\mathrm{c}}$), which is determined by the effective population time τ_{c} of partly

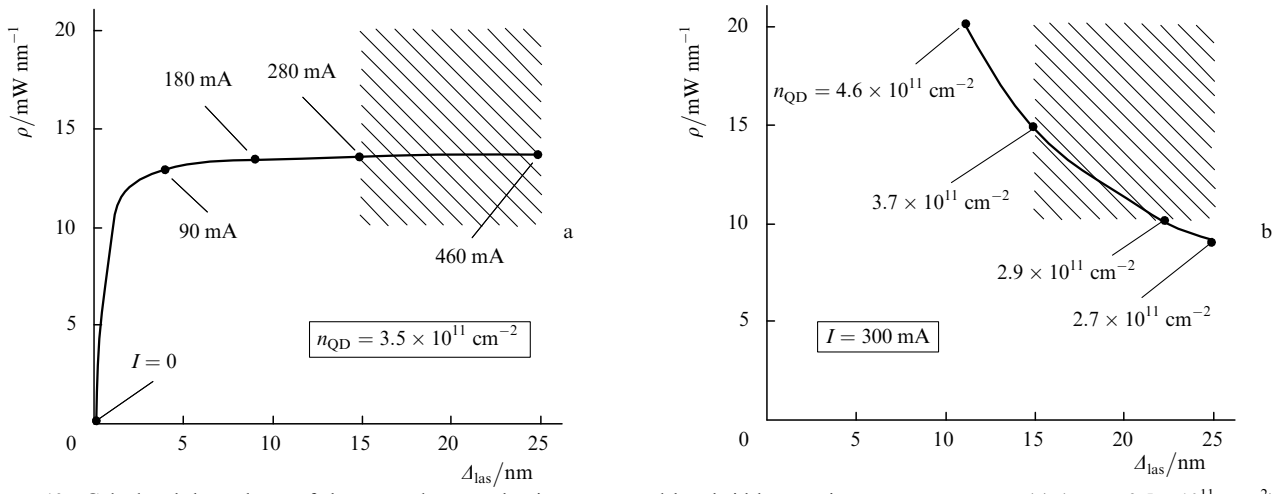

Figure 10. Calculated dependence of the spectral power density on spectral bandwidth at various pump currents I (a) ($n_{QD} = 3.5 \times 10^{11}$ cm^{-2}) or various effective surface densities n_{QD} of a QD array (b) ($I = 300$ mA).

populated QD ground state [50, 56]. In turn, the average spectral power density is the ratio of the output laser power, dependent on the pump current, to the laser linewidth.

Effect of the pump current on the spectral width and the spectral power density is illustrated in Fig. 10a. As the pump current is increased, the bandwidth of the emission spectrum increases due to the spectral hole burning effect. The output power also increases. At relatively low currents (< 90 mA), the output power increases faster than the spectral width, so that the spectral power density increases. At high currents (> 180 mA), the output power and the spectral width are linearly related with each other. As a result, the spectral power density saturates at a certain level, which is 13 mW nm^{-1} for the given set of parameters. One can see that the spectral width can exceed 15 nm provided that the pump current exceeds 280 mA. The results of the calculations show that to achieve simultaneously large laser linewidths and high spectral power densities, it is necessary to use high pump currents.

Laser parameters (the surface density of a QD array, the length and the width of a laser stripe, the pump current) affect the spectral bandwidth and the spectral power density both directly, through their effect on a total number N_{QD} of QDs in the active region, and indirectly, by means of their impact on a threshold current density and a differential quantum efficiency. If the total number of QDs in the laser active region decreases in one or another way, the spectral width of emission increases, while the spectral power density decreases. As an example, Fig. 10b illustrates the influence of the surface density of a QD array. One can see that if the effective surface density of QDs is properly selected [within the $(2.9 - 3.7) \times 10^{11}$ cm^{-2} range for the parameters assumed in the calculations], the width of a QD laser emission spectrum may exceed 15 nm, while the spectral power density may simultaneously be higher than 10 mW nm^{-1}. At the same time, at lower QD surface densities the spectral power density may be insufficiently high, whereas at higher values of n_{QD} the spectral bandwidth may be insufficient. Taking into account a usual surface density of self-organised QDs, which is about 5×10^{10} cm^{-2}

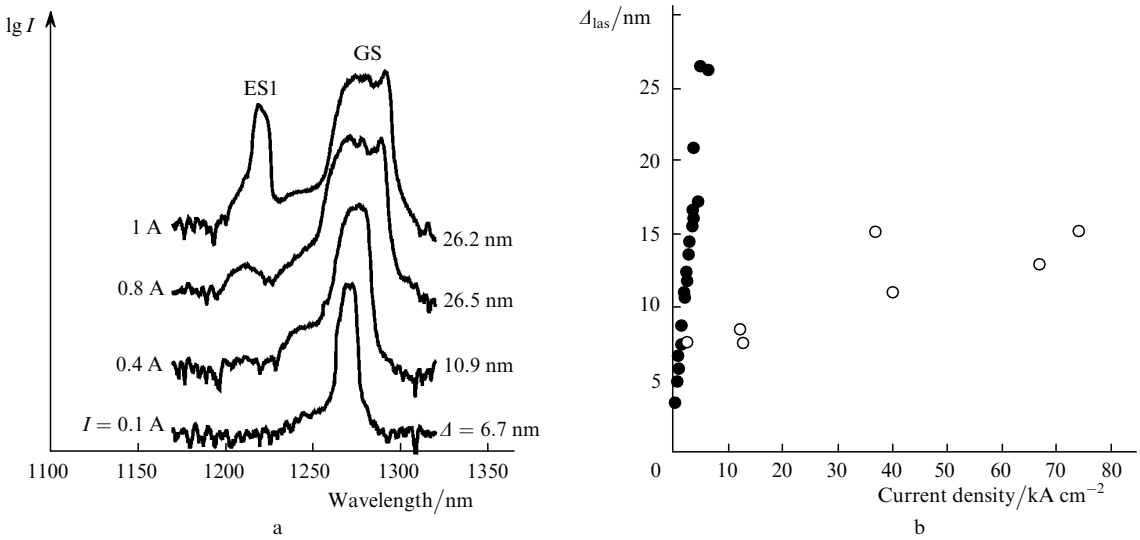

Figure 11. Room-temperature lasing emission spectra taken at different currents with 2-nm spectral averaging for a 4-μm broad and 2-mm long laser comprising 7 layers of QDs (a); dependence of the lasing emission linewidth at half maximum on the pump current density for Fabry–Perot lasers based on quantum dots (solid circles) or quantum wells (open circles) (b).

per QD layer, optimum values of n_{QD} corresponds to approximately 7 layers of QDs in the laser's active region.

In QD lasers properly optimised in accordance with the predictions of the above model, lasing emission spectra were experimentally demonstrated to have spectral widths of 17 nm [55] and 26 nm [57] with an average spectral power density of 10.2 – 10.4 mW nm^{-1}. Evolution of lasing spectra with a drive current of a laser diode is shown in Fig. 11a.

Note that broadening of the laser emission spectrum is also found in QW lasers. However, unlike QD lasers, the line broadening in QWs occurs at much higher current densities. For example, the full width at half-maximum of the line of a 1.04-μm InGaAs/GaAs QW laser was ~13 nm at a pump current of 67 kA cm^{-2} [58]. A similar result was obtained in Ref. [59] for a 1.55-μm QW laser on a InP substrate as well where the full width at half-maximum was ~15 nm at a pump current of 74 kA cm^{-2}. Dependences of the laser linewidth on a pump current density are compared in Fig. 11b for multifrequency QD and QW lasers. One can see from the data presented that a 15-nm broad linewidth requires a 20 times less pumping level (about 3 kA cm^{-2}) in the case of QDs as compared to that of QWs. To a considerable degree this behavior is caused by a lower density of states of a QD array.

One can see from the data presented in Fig. 11a that an additional group of longitudinal modes appears in a lasing spectrum of a QD laser at high pump currents. Its spectral position corresponds to a wavelength of the excited-state optical transition ($\lambda \sim 1.22$ μm). As a pump current is further increased, a power of the ground-state emission and its spectral width remain virtually unchanged, whereas a subsequent increment of an emission power is caused by the excited-state optical transition. Simultaneous lasing involving two quantum states in QD lasers is associated with a gradual increase in the carrier concentration on the QD excited state with increasing the pumping, which in turn is caused by a relatively low rate of the ground-state population process [50, 60].

Thus, both broadening of the ground-state lasing spectrum and excitation of the excited-state lasing band have the same cause. However, in most cases the spectral bands of these two optical transitions are well separated from each other, so that a lasing spectrum usually comprises two pronounced maxima. At the same time, it is highly desired for practical applications to produce a lasing spectrum having a nearly uniform distribution of its power density across the entire spectral interval. It may be achieved if the optical transitions of the ground-state and the excited-state overlap each other. In turn, this situation may be realised if an inhomogeneous broadening width is significantly large. It has been demonstrated in Ref. [61] that an array of QDs can be formed by a periodic monolayer deposition of InAs/GaAs pairs which results in a width of a luminescence spectrum of 82 nm and a width of a lasing spectrum of 20 nm owing to concurrent lasing through two overlapping optical transitions. A disadvantage of such an active region is that its wavelength is too short (~1.17 μm) because of the formation method.

The density of states of a QD array may be additionally broadened even in case of longer-wavelength QDs provided that a stacked QD array is deposited so that some parameter affecting a spectral position of a central wavelength is gradually varied from layer to layer [62]. In particular, a width of an InGaAs layer that covers QDs may be used as such a parameter. The use of this method allowed us to reach a lasing spectral width of 75 nm at half maximum [63]. A laser's active region comprised three groups of InAs/InGaAs QDs with various thicknesses of InGaAs cap layers (1.5, 3 or 4 nm). Figure 12 shows a lasing spectrum at a 3.7-A current (18.5 kA cm^{-2}) superimposed on an active region electroluminescence spectrum detected at a low excitation. A comparison of the spectra reveals that the lasing spectrum comprises spectral components arisen from both the ground-state (GS) and the excited-state (ES) optical transitions. Overlap of these transitions caused by intentional inhomogeneous broadening and approximate equalisation of their intensities at a certain pump level results in a larger spectral width and a high degree of uniformity of a spectral power density. A total emission power is 750 mW and an average spectral power density is 10 mW nm^{-1}, whereas a spectral uniformity of the power density is 4.5 dB. Insert of Fig. 12 depicts a high-resolution lasing spectrum measured under continuous-wave operation. The spectrum consists of a series of longitudinal Fabry – Perot modes. This finding confirms that spectral broadening originates from excitation of additional modes whereas each of modes remains quite narrow (about 0.015 nm).

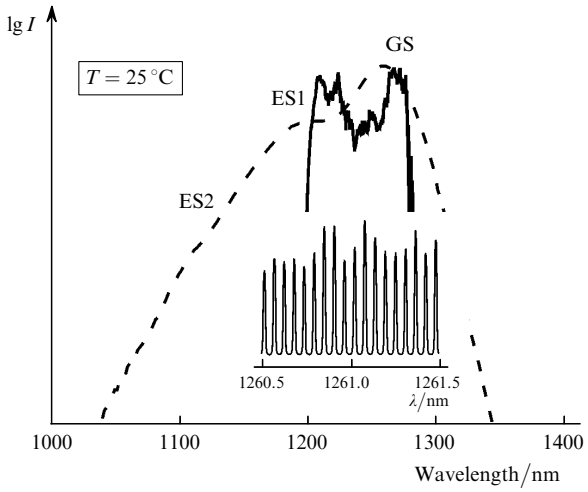

Figure 12. Electroluminescence (50 A cm^{-2}) (dashed curve) and lasing (3.7 A) (solid curve) spectra taken at 25 °C for a laser comprising a QD array with intentional inhomogeneous broadening. Insert: part of the lasing spectrum taken in the cw regime with a 0.01-nm spectral resolution.

5. Broadband laser diodes for wavelength-division-multiplexing systems

Simultaneous transmission of several information channels at different carrier wavelengths along one optical waveguide results in significant enhancement of an optical communication line capacity. This technique, called the wavelength-division-multiplexing (WDM), currently utilises an array of single-frequency lasers as an optical source, for example an array of distributed feedback (DFB) lasers (Fig. 13a). However, fabrication complexity of a DFB laser multiplied by their large number results in a high cost of such systems and impedes their wide applications for data communication over short- and ultrashort distances. Moreover, a wavelength of every optical channel is individually deter-

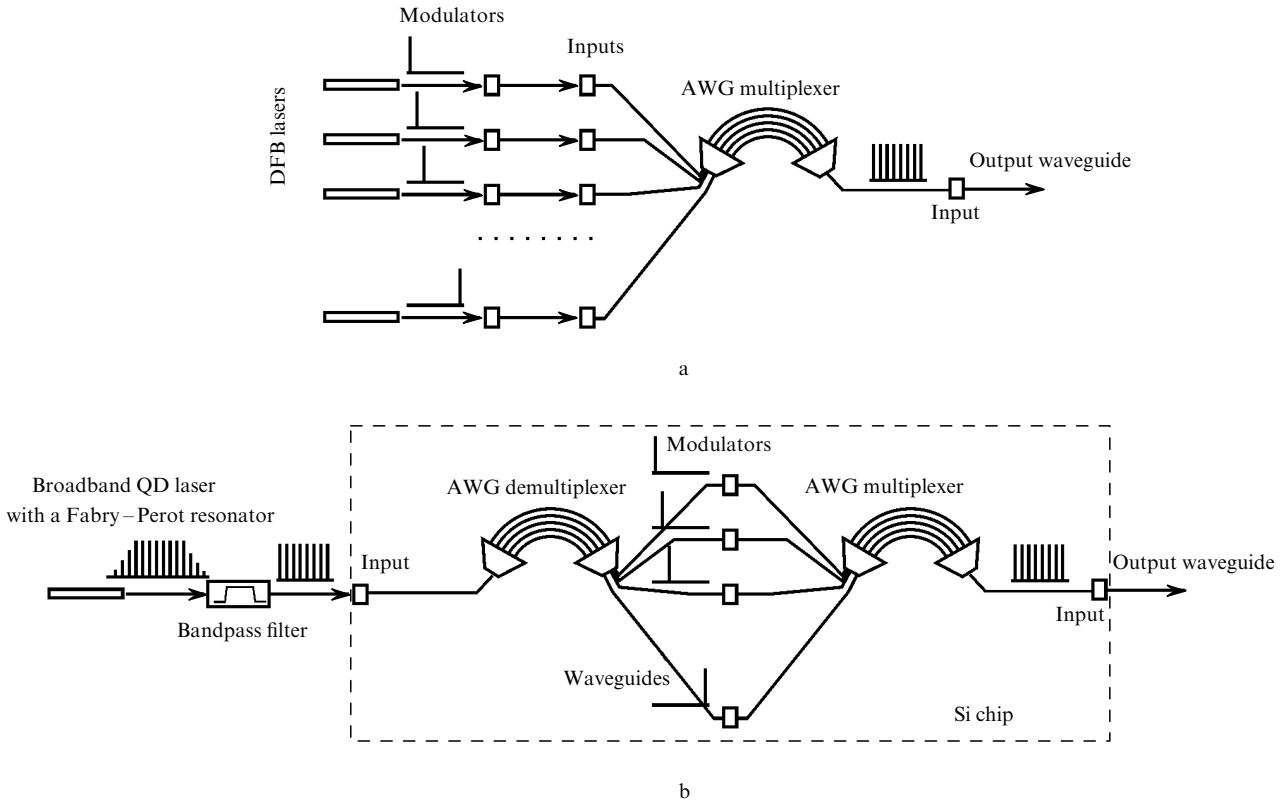

Figure 13. Layout of an optical wavelength-division-multiplexing transmitter based on either an array of single-frequency lasers (a) or a broadband multifrequency laser (b).

mined for each single-frequency laser. This leads to necessity of their individual stabilisation and tracking and makes it difficult to arrange an array of equally spaced wavelengths. The system of this kind also suffers from necessity to couple emission of every laser into an individual waveguide. As a number of optical channels increases all the aforementioned disadvantages of the conventional optical source are aggravated.

In this respect, the use of a multifrequency laser diode seems to be an attractive alternative because of its simplicity and cheapness in fabrication. This approach mitigates a required precision of wavelengths of many single-frequency lasers because a spectral separation of channels, which are Fabry–Perot modes, is naturally predetermined by the only parameter, i.e. the cavity length. Moreover, all the channels can be simultaneously stabilised, and the stability of carrier wavelengths of all channels can be tracked by using a wavelength of one channel.

It should be noted that a spectral spacing between adjacent longitudinal modes $\Delta f = c/(2nL)$ at usual lengths of Fabry–Perot lasers conforms well to modern requirements to a frequency spacing in wavelength-division-multiplexing systems. For example, an intermode spacing of 50 GHz needs a cavity length of 0.9 mm. Assuming such spectral spacing, different wavelengths, that correspond to various cavity modes, may be spectrally divided by available optical means of demultiplexing (e.g., by means of an arrayed waveguide grating), individually encoded by an external modulator and thus be used as independent optical data-bearing channels. Subsequent multiplexing enables coupling all the channels into a transmitting fiber or a planar waveguide. A possible layout of a WDM transmitter based on a broadband multifrequency laser is sketched in Fig. 13b [64].

The most preferable scheme is that where all external optical means (multiplexers, demultiplexer, modulators) are monolithically integrated on a single silicon chip and connected to each other by planar optical waveguides, e.g. SiGe-based. Owing to its small footprint, a laser diode may be placed directly onto the silicon chip. Coupling of a laser emission into a waveguide may be realised for example in vertical direction through a substrate [65]. A 90° turn of a part of the laser emission may be implemented e.g. by means of a monolithically integrated second-order grating formed by etching of trenches placed normal to the laser stripe. In an alternative solution, the laser emission may be edge-coupled into the waveguide by conventional optical means both directly and through an intermediate optical fiber. In the latter case the laser diode may be placed aside from the silicon optoelectronic chip. This may be useful for some purposes, e.g. to prevent an overlap of thermal fields. A 64-channel optical transmitter with a 50-GHz inter-channel interval requires a spectral band of a laser emission of about 15 nm in width. As it was demonstrated above, this spectral width of a laser emission is quite attainable by means of lasers based on self-organised quantum dots. The optical source may further comprise a spectral pass-filter in order to select a required number of channels out of a broader spectrum of the laser emission [66].

The most essential issue to be addressed in detail is a noise performance of such transmitting system which is quantitatively expressed by a bit error rate (BER). In its turn, the BER depends on a system signal-to-noise ratio determined by shot noise and thermal noise of a photo-

detector and to a great degree by noise of an optical intensity. Assuming equal probabilities of sending a '0'-bit and a '1'-bit and equal noise at both levels, the lowest possible bit error rate corresponding to an optimum decision level of the detector system is expressed by the following equation [67]: $\mathrm{BER} = 0.5\mathrm{erfc}\,(Q/\sqrt{2})$, where $\mathrm{erfc}(x)$ is a complementary error function; $Q = (v_1 - v_0)/(\sigma_1 + \sigma_0)$; $v_{1,0}$ and $\sigma_{1,0}$ are mean signal intensities and root-mean-square deviations at 1 and 0 levels, respectively. It is usually considered that transmission is error-free if BER does not exceed 10^{-12}. It can be revealed from the data presented in Fig. 14a that error-free transmission requires at least the Q-factor of no worse than 8.5 dB.

The Q-factor of an optical transmission system depends on a maximum optical power P impinging on a detector, an extinction ratio ER of optical signal modulation, a detector responsivity R_{sp}, an electrical bandwidth B_e of a detector circuit, equivalent thermal noise i_{th} of the detector, and relative intensity noise $\langle \mathrm{RIN} \rangle$ of the optical power averaged over the B_e frequency interval. Figure 14b shows calculation results for a dependence of the Q-factor on the optical signal power at various values of the extinction ratio for the 10-GHz frequency interval assuming the following parameters: $R_{sp} = 0.5$ A W^{-1}, $i_{th} = 10$ pA Hz$^{-1/2}$, $\langle \mathrm{RIN} \rangle = -125$ dB Hz^{-1}. One can see that a value of the Q-factor, which satisfies the condition of error-free transmission, requires an optical power of more than -10 dBm and an extinction ratio of at least 5 dB.

Note that a responsivity of 0.71 – 0.73 A W^{-1} has been demonstrated in 1.3-μm photodetecors of metal – semiconductor – metal type based on InGaAs/InP heterostructures [68]. Taking into account that a standard single-mode optical fiber is characterised by an attenuation coefficient of less than 0.4 dB km^{-1} in the 1.3-μm spectral band and assuming that laser-to-fiber coupling loss is -3 dB (a 75 % – 80 % coupling efficiency has been demonstrated for 1.3 μm spatially single-mode Fabry – Perot lasers [69]), transmission over a distance of about 10 km requires a laser emission output power of about -3 dBm per channel, i.e. 0.5 mW. Assuming a 0.2-nm spectral separation between longitudinal modes, an average spectral power density of the laser emission should exceed 3 mW nm^{-1}. Thus, an average spectral power density of 10 mW nm^{-1} achievable in a multifrequency QD laser provides a threefold margin with respect to the required power level and enables compensating any unforeseen loss associated with e.g. fiber bending or loss in a modulator. In case of optical transmission over an ultrashort distance (for example, within an optoelectronic integrated circuit) a propagation-related signal attenuation is nearly negligible. However, in this case one should take into account a lower coupling efficiency into a planar waveguide as well as a lower responsivity of a monolithically integrated photodetector.

One can see from Fig. 14b that the Q-factor becomes independent of the power level at a sufficiently high optical power because it is completely determined by the optical signal noise. In this case the bit error rate only depends on the extinction ratio and the integrated relative intensity noise of the optical signal: $\mathrm{BER} \approx 0.5\mathrm{erfc}\,(m/\sqrt{2\langle \mathrm{RIN} \rangle B_e})$, where $m = (\mathrm{ER} - 1)/(\mathrm{ER} + 1)$. It is evident from calculation

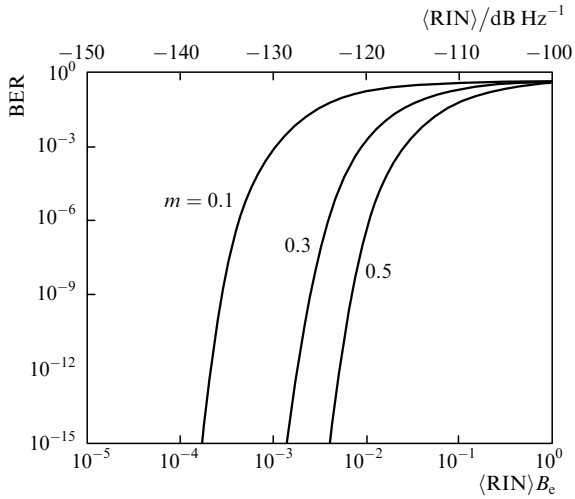

Figure 15. Dependence of the bit error rate on the integrated relative intensity noise of an optical signal at various values of the amplitude modulation index (upper scale corresponds to the average relative intensity noise for $B_e = 10$ GHz).

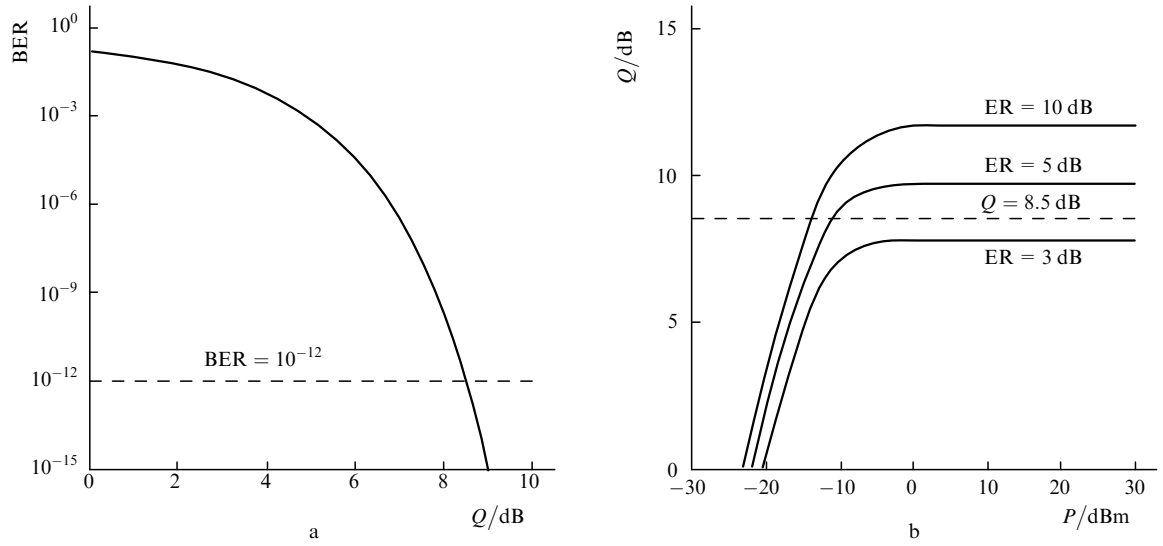

Figure 14. Dependence of the bit error rate on Q-factor (assuming an equal probability of sending a '0'-bit and a '1'-bit) (a); dependence of the Q-factor on the optical signal power at different extinction ratios (b).

results of Fig. 15 that for error-free data transmission along an optical channel with an amplitude modulation index $m = 0.5$ (ER = 4.7 dB) an integrated relative intensity noise of the optical signal $\langle \mathrm{RIN} \rangle B_e$ should be better than 0.5 %. For the 10-GHz frequency interval this corresponds to an average relative intensity noise $\langle \mathrm{RIN} \rangle$ of -125 dB Hz^{-1} or lower.

The aforementioned value of the extinction ratio can be easily achieved by means of external modulation. At the same time, attainment of a low relative intensity noise seems to be problematic with using conventional laser sources. In a single-frequency laser with a high side mode suppression ratio (> 40 dB) the relative intensity noise is found to be acceptably low for its use in an optical communication system. As the side mode suppression ratio increases (in other words, as a laser comes to the multifrequency regime), the relative intensity noise of a given longitudinal mode increases up to an unacceptably high level (see, e.g., [70]). This behavior is caused by mode beating (or mode partition) effect that manifests itself through a random redistribution of an emission intensity between co-existing longitudinal modes of the laser spectrum. Therefore, a spectral division of a quantum well laser emission into several spectral channels, even it is feasible by present means of wavelength demultiplexing, does not permit realising error-free optical transmission.

It was found that a dissimilar situation takes place in semiconductor lasers, whose active medium is characterised by a pronounced effect of nonlinear gain saturation, or, generally speaking, in lasers, in which the relaxation oscillations are strongly damped. For example, a reduction of a main mode relative intensity noise of a two-frequency laser, if non-linear gain saturation is taken into account, was demonstrated in [71]. A similar conclusion for a multi-frequency laser as well has been drawn in Ref. [72] where a behavior of 21 longitudinal modes has been numerically simulated: strong damping of the relaxation oscillations suppresses fluctuations of a photon density in a laser cavity reducing a relative intensity noise of a given longitudinal mode.

It was mentioned above that the relaxation oscillations in QD lasers are strongly damped. This peculiarity is caused by a high gain compression factor ε. Gain compression, also known as nonlinear gain saturation or self-saturation, describes how an optical gain of an active region decreases with increasing a photon density. A value of ε in QD lasers was found to be about 5×10^{-16} cm^3 [73, 74] which is at least one order of magnitude greater than values measured in QW lasers. In order to explain a high gain compression factor ε in QD lasers it was suggested that its high values are associated with either a long carrier capture time to QD lasing states [75] or a differential gain reduction of a QD active region as a threshold gain approaches the saturated gain [73]. It was also shown in Ref. [76] that Coulomb interaction in a QD laser leads to strong damping of the relaxation oscillations.

It has been previously demonstrated that a relative intensity noise of a total optical power of a multifrequency QD laser is about -159 dB Hz^{-1} in the frequency range to 10 GHz [77, 78]. However, the intensity stability of a given longitudinal mode was disputable because a modal intensity in a semiconductor laser can significantly fluctuate even if the total power remains stable (see, e.g., [79]). We have experimentally demonstrated, for the first time, that a relative intensity noise of a spectrally filtered longitudinal mode of a multi-frequency QD laser can be much lower than typical values of quantum well lasers [80].

Figure 16a shows a part of an emission spectrum of a multifrequency QD laser superimposed to a spectrum of one spectrally filtered longitudinal mode. An external Fabry–Perot etalon was used in the experiment for spectral filtering. In this case a side mode suppression ratio of 19–20 dB was achieved. Figure 16b depicts a relative intensity noise spectrum for a spectrally filtered longitudinal mode (1265.5 nm) of the multifrequency QD laser measured in the 1-MHz–10-GHz frequency interval. The relative inten-

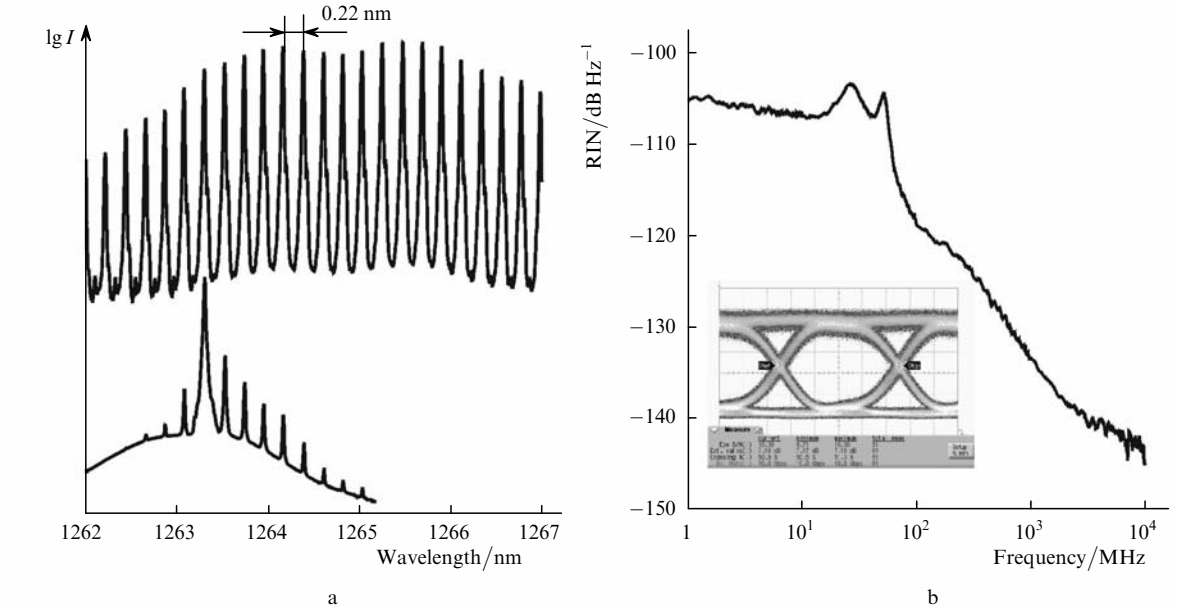

Figure 16. Part of an emission spectrum of a multifrequency QD laser and a spectrum of one spectrally filtered longitudinal mode (1263.3 nm) (a); relative intensity noise spectrum for a spectrally filtered longitudinal mode (1265.5 nm) of the multifrequency QD laser (b). Insert: eye diagram generated by a 10-Gb s^{-1} external modulation for one filtered longitudinal mode of the multifrequency QD laser.

sity noise was integrated over this frequency interval to be 0.21%, so that an average value $\langle RIN \rangle$ is -126 dB Hz^{-1}. In accordance with the calculation results (Fig. 15), this value is sufficiently low for error-free optical transmission assuming that an extinction ratio is better than 5 dB.

An intensity of a spectrally filtered longitudinal mode of the quantum dot laser was modulated by a $2^{31}-1$ pseudorandom binary sequence with a 10-Gb s^{-1} rate by an external $LiNbO_3$ modulator. Insert in Fig. 16b shows an example of an eye pattern at a -3-dBm received power at a photodetector. The extinction ratio was 7 dB whereas the Q-factor was measured to be 9.7 – 10.3 dB. For this case, as well as for nine other longitudinal modes, a bit error rate of less than 10^{-13} was demonstrated. To the best of our knowledge, this is the first experimental demonstration of a high-speed error-free transmission using spectral filtering of emission of a multifrequency laser.

6. Conclusions

Semiconductor QDs have attracted attention long ago because of the ultimate case of size quantisation. However, over a long period of time QD lasers were far from their practical use being under pressure of the well-developed technology of quantum well lasers. Development of wavelength control methods in quantum dots, which resulted in achievement of lasing operation in the 1.2 – 1.3 μm wavelength interval, has radically changed the situation. Quantum dot lasers have got their own niche beyond the reach of quantum well lasers. Wavelengths of this spectral window are, on the one hand, too short for quantum wells on InP and, on the other hand, too long for quantum wells on GaAs, whereas these wavelengths seem to be optimal for InAs/InGaAs QDs. Large localisation energy in such a QD active region, which suppresses population of the matrix states by charge carriers, gives an opportunity to reach extremely low threshold currents and a high temperature stability of laser characteristics. At the same time, this wavelength interval is favourable for optical fiber communication as well as ultrashort range optical communication.

Relatively low population rate of electronic states that contribute to lasing and high non-linear gain coefficients in QDs, which lead to strong damping of the relaxation oscillations, prevent QD lasers from reaching certain advantages over quantum wells in respect to the cutoff frequency of direct modulation. On the other hand, this feature of the active region results in a unique peculiarity of QD lasers, which consists in a low relative intensity noise of longitudinal modes in multifrequency lasing regime. This opens up wide possibilities for applications of QD lasers as optical sources in multichannel communication systems, which is supported by another QD peculiarity that resides in their capability of simultaneous emitting many longitudinal modes. It is most likely that one may foresee significant progress in the development of QD laser sources and systems based on them which are specifically optimised for WDM.

Acknowledgements. This work was supported by SANDiE and ZODIAC projects of European Commissions, Project N.P.2.1.1.2215 of the Russian Ministry of Education and Science, the President's Grant MD-3858.2007.2 (A.E.Z.), Program of Presidium of RAS 'Quantum nanostructure', Program of Phys. Dep. of RAS 'Coherent optical emission of semiconductor compounds and structures'.

References

1. US patent 6,770,134 dated 03.08.2004.
2. Temkin H., Coblentz D., Logan R.A., van der Ziel J.P., Tanbun-Ek T., Yadvish R.D., Sergent A.M. *Appl. Phys. Lett.*, **62**, 2402 (1993).
3. Takemasa K., Munakata T., Kobayashi M., Wada H., Kamijoh T. *Electron. Lett.*, **34**, 1231 (1998).
4. Schaefer F., Mayer B., Reithmaier J.P., Forchel A. *Appl. Phys. Lett.*, **73**, 2863 (1998).
5. Kondow M., Uomi K., Niwa A., Kitatani T., Watahiki S., Yazawa Y. *Jpn. J. Appl. Phys.*, **35**, 1273 (1996).
6. Sato S., Satoh S. *Jpn. J. Appl. Phys.*, **38**, L990 (1999).
7. Arakawa Y., Sakaki H. *Appl. Phys. Lett.*, **40**, 939 (1982).
8. Goldstein L., Glas F., Marzin J.Y., Charasse M.N., Le Roux G. *Appl. Phys. Lett.*, **47**, 1099 (1985).
9. Egorov A.Yu., Zhukov A.E., Kop'ev P.S., Ledentsov N.N., Maximov M.V., Ustinov V.M., Tsatsul'nikov A.F., Alferov Zh.I., Fedorov D.L., Bimberg D. *Semiconductors*, **30**, 707 (1996).
10. Mukai K., Ohtsuka N., Sugawara M., Yamazaki S. *Jpn. J. Appl. Phys.*, **33**, L1710 (1994).
11. Mirin R.P., Ibbetson J.P., Nishi K., Gossard A.C., Bowers J.E. *Appl. Phys. Lett.*, **67**, 3795 (1995).
12. Huffaker D.L., Deppe D.G. *Appl. Phys. Lett.*, **73**, 520 (1998).
13. Zhukov A.E., Kovsh A.R., Egorov A.Yu., Maleev N.A., Ustinov V.M., Volovik B.V., Maximov M.V., Tsatsul'nikov A.F., Ledentsov N.N., Shernyakov Yu.M., Lunev A.V., Musikhin Yu.G., Bert N.A., Kop'ev P.S., Alferov Zh.I. *Semiconductors*, **33**, 153 (1999).
14. Volovik B.V., Tsatsul'nikov A.F., Bedarev D.A., Egorov A.Yu., Zhukov A.E., Kovsh A.R., Ledentsov N.N., Maximov M.V., Maleev N.A., Musikhin Yu.G., Suvorova A.A., Ustinov V.M., Kop'ev P.S., Alferov Zh.I. *Semiconductors*, **33**, 901 (1999).
15. Egorov A.Yu., Zhukov A.E., Kop'ev P.S., Ledentsov N.N., Maximov M.V., Ustinov V.M. *Semiconductors*, **28**, 809 (1994).
16. Kirstaedter N., Ledentsov N.N., Grundmann M., Bimberg D., Ustinov V.M., Ruvimov S.S., Maximov M.V., Kop'ev P.S., Alferov Zh.I., Richter U., Werner P., Gosele U., Heydenreich J. *Electron. Lett.*, **30**, 1416 (1994).
17. Zhukov A.E., Kovsh A.R., Ustinov V.M., Egorov A.Yu., Ledentsov N.N., Tsatsul'nikov A.F., Maximov M.V., Shernyakov Yu.M., Kopchatov V.I., Lunev A.V., Kop'ev P.S., Bimberg D., Alferov Zh.I. *Semicond. Sci. Technol.*, **14**, 118 (1999).
18. Salhi A., Martiradonna L., Visimberga G., Tasco V., Fortunato L., Todaro M.T., Cingolani R., Passaseo A., De Vittorio M. *IEEE Photon. Technol. Lett.*, **18**, 1735 (2006).
19. Amano T., Aoki S., Sugaya T., Komori K., Okada Y. *IEEE J. Sel. Top. Quantum Electron.*, **13**, 1273 (2007).
20. Alferov Zh.I., Bert N.A., Egorov A.Yu., Zhukov A.E., Kop'ev P.S., Kosogov A.O., Krestnikov I.L., Ledentsov N.N., Lunev A.V., Maksimov M.V., Sakharov A.V., Ustinov V.M., Tsatsul'nikov A.F., Shernyakov Yu.M., Bimberg D. *Semiconductors*, **30**, 194 (1996).
21. Ustinov V.M., Egorov A.Yu., Kovsh A.R., Zhukov A.E., Maksimov M.V., Tsatsul'nikov A.F., Gordeev N.Yu., Zaitsev S.V., Shernyakov Yu.M., Bert N.A., Kop'ev P.S., Alferov Zh.I., Ledentsov N.N., Bohrer J., Bimberg D., Kosogov A.O., Werner P., Gosele U.J. *Cryst. Growth*, **175/176**, 689 (1997).
22. Huffaker D.L., Park G., Zou Z., Shchekin O.B., Deppe D.G. *Appl. Phys. Lett.*, **73**, 2564 (1998).

23. Lester L.F., Stinz A., Li H., Newell T.C., Pease E.A., Fuchs B.A., Malloy K.J. *IEEE Photon. Technol. Lett.*, **11**, 931 (1999).
24. Zhukov A.E., Kovsh A.R., Maleev N.A., Mikhrin S.S., Ustinov V.M., Tsatsul'nikov A.F., Maximov M.V., Volovik B.V., Bedarev D.A., Shernyakov Yu.M., Kop'ev P.S., Alferov Zh.I., Ledenstov N.N., Bimberg D. *Appl. Phys. Lett.*, **75**, 1926 (1999).
25. Zhukov A.E., Kovsh A.R., Ustinov V.M., Shernyakov Yu.M., Mikhrin S.S., Maleev N.A., Kondrat'eva E.Yu., Livshits D.A., Maximov M.V., Volovik B.V., Bedarev D.A., Musikhin Yu.G., Ledentsov N.N., Kop'ev P.S., Alferov Zh.I., Bimberg D. *IEEE Photon. Technol. Lett.*, **11**, 1345 (1999).
26. Maximov M.V., Gordeev N.Yu., Novikov I.I., Shernyakov Yu.M., Zhukov A.E., Ustinov V.M., Krestnikov I.L., Livshits D.A., Mikhrin S.S. *Intern. Workshop on Quantum Dots and Laser Applications* (Wroclav, Poland, July 12 – 24, 2007) QDLPII.1.
27. Mikhrin S.S., Zhukov A.E., Kovsh A.R., Maleev N.A., Vasil'ev A.P., Semenova E.S., Ustinov V.M., Kulagina M.M., Nikitina E.V., Soshnikov I.P., Shernyakov Yu.M., Livshits D.A., Kryjanovskaya N.V., Sizov D.S., Maximov M.V., Tsatsul'nikov A.F., Ledentsov N.N., Bimberg D., Alferov Zh.I. *Semiconductors*, **36**, 1315 (2002).
28. Zhukov A.E., Kovsh A.R., Ustinov V.M., Alferov Zh.I. *Las. Phys.*, **13**, 319 (2003).
29. Kovsh A.R., Maleev N.A., Zhukov A.E., Mikhrin S.S., Vasil'ev A.P., Shernyakov Yu.M., Maximov M.V., Livshits D.A., Ustinov V.M., Alferov Zh.I., Ledentsov N.N., Bimberg D. *Electron. Lett.*, **38**, 1104 (2002).
30. Huang X., Stinz A., Hains C.P., Liu G.T., Cheng J., Malloy K.J. *Electron. Lett.*, **36**, 41 (2000).
31. Park G., Shchekin O.B., Csutak S., Huffaker D.L., Deppe D.G. *Appl. Phys. Lett.*, **75**, 3267 (1999).
32. Park G., Shchekin O.B., Huffaker D.L., Deppe D.G. *IEEE Photon. Technol. Lett.*, **12**, 230 (2000).
33. Chand N., Becker E.E., van der Zeil J.P., Chu S.N.G., Dutta N.K. *Appl. Phys. Lett.*, **58**, 1704 (1991).
34. Turner G.W., Choi H.K., Manfra M.J. *Appl. Phys. Lett.*, **72**, 876 (1998).
35. US patent 7,043,106 dated 09.05.2006.
36. Huang X., Stintz A., Li H., Lester L.F., Cheng J., Malloy K.J. *Appl. Phys. Lett.*, **78**, 2825 (2001).
37. Thompson M.G., Marinelli C., Tan K.T., Williams K.A., Penty R.V., White I.H., Kaiander I.N., Sellin R.L., Bimberg D., Kang D.-J., Blamire M.G., Visinka F., Jochum S., Hansmann S. *Electron. Lett.*, **39**, 1121 (2003).
38. Gubenko A., Livshits D., Krestnikov I., Mikhrin S., Kozhukhov A., Kovsh A., Ledentsov N., Zhukov A., Portnoi E. *Electron. Lett.*, **41**, 1124 (2005).
39. Kuntz M., Fiol G., Lammlin M., Bimberg D., Kovsh A.R., Mikhrin S.S., Kozhukhov A.V., Ledentsov N.N., Schubert C., Ustinov V.M., Zhukov A.E., Shernyakov Yu.M., Jacob A., Umbach A. *Int. Symp. «Nanostructures: Physics and Technology»* (St Petersburg, June 20 – 25, 2005) Paper LOED.01o.
40. Kuntz M., Fiol G., Laemmlin M., Schubert C., Kovsh A.R., Jacob A., Umbach A., Bimberg D. *Electron. Lett.*, **41**, 244 (2005).
41. Ishida M., Hatori N., Otsubo K., Yamamoto T., Nakata Y., Ebe H., Sugawara M., Arakawa Y. *Electron. Lett.*, **43**, 219 (2005).
42. Kovsh A.R., Zhukov A.E., Odnoblyudov M.A., Egorov A.Yu., Ustinov V.M., Ledentsov N.N., Maksimov M.V., Tsatsul'nikov A.F., Gordeev N.Yu., Zaitsev S.V., Kop'ev P.S., in *«Advanced Electronic Technologies and Systems Based on Low-Dimensional Quantum Devices»*. Ed. by M. Balkanski, N. Andreev (Dordrecht: Kluwer Acad. Publ., 1998) p. 207.
43. Zhukov A.E., Ustinov V.M., Egorov A.Yu., Kovsh A.R., Tsatsul'nikov A.F., Ledentsov N.N., Zaitsev S.V., Gordeev N.Yu., Kop'ev P.S., Alferov Zh.I. *Jpn. J. Appl. Phys.*, **36**, 4216 (1997).
44. Zhukov A.E., Kovsh A.R., Mikhrin S.S., Vasil'ev A.P., Semenova E.S., Maleev N.A., Ustinov V.M., Kulagina M.M., Nikitina E.V., Soshnikov I.P., Shernyakov Yu.M., Livshits D.A., Kryjanovskaya N.V., Sizov D.S., Maximov M.V., Tsatsul'nikov A.F., Ledentsov N.N., Bimberg D., Alferov Zh.I. *Physica E*, **17**, 589 (2003).
45. Shchekin O.B., Deppe D.G. *Appl. Phys. Lett.*, **80**, 3277 (2002).
46. Fathpour S., Mi Z., Bhattacharya P., Kovsh A.R., Mikhrin S.S., Krestnikov I.L., Kozhukhov A.V., Ledentsov N.N. *Appl. Phys. Lett.*, **85**, 5164 (2004).
47. Shchekin O.B., Ahn J., Deppe D.G. *Electron. Lett.*, **38**, 712 (2002).
48. Krestnikov I., Livshits D., Mikhrin S., Kozhukhov A., Kovsh A., Ledentsov N., Zhukov A. *Electron. Lett.*, **41**, 1330 (2005).
49. Benisty H., Sotomayor-Torres C.M., Weisbuch C. *Phys. Rev. B*, **44**, 10945 (1991).
50. Zhukov A.E., Kovsh A.R., Livshits D.A., Ustinov V.M., Alferov Zh.I. *Semicond. Sci. Technol.*, **18**, 774 (2003).
51. Sugawara M., Mukai K., Nakata Y. *Appl. Phys. Lett.*, **74**, 1561 (1999).
52. Grundmann M., Heinrichsdorf F., Ledentsov N.N., Ribbat C., Bimberg D., Zhukov A.E., Kovsh A.R., Maximov M.V., Shernyakov Yu.M., Ustinov V.M., Alferov Zh.I. *Jpn. J. Appl. Phys.*, **39**, 2341 (2000).
53. Mikhrin S.S., Zhukov A.E., Kovsh A.R., Maleev N.A., Ustinov V.M., Shernyakov Yu.M., Kayander I.N., Kondrat'eva E.Yu., Livshits D.A., Tarasov I.S., Maksimov M.V., Tsatsul'nikov A.F., Ledentsov N.N., Kop'ev P.S., Bimberg D., Alferov Zh.I. *Semiconductors*, **34**, 119 (2000).
54. Livshits D.A., Kovsh A.R., Zhukov A.E., Maleev N.A., Mikhrin S.S., Vasil'ev A.P., Nikitina E.V., Ustinov V.M., Ledentsov N.N., Lin G., Chi J. *Tech. Phys. Lett.*, **30**, 9 (2004).
55. Zhukov A.E., Kovsh A.R., Nikitina E.V., Ustinov V.M., Alferov Zh.I. *Semiconductors*, **41**, 606 (2007).
56. Mukai K., Ohtsuka N., Shoji H., Sugawara M. *Appl. Phys. Lett.*, **68**, 3013 (1996).
57. Zhukov A.E., Ustinov V.M., Kovsh A.R. *15th Int. Symp. «Nanostructures: Physics and Technology»* (Novosibirsk, Russia, 25 – 29 June, 2007).
58. Slipchenko S.O., Sokolova Z.N., Pikhtin N.A., Borschev K.S., Vinokurov D.A., Tarasov I.S. *Semiconductors*, **40**, 990 (2006).
59. Vinokurov D.A., Kapitonov V.A., Lyutetskii A.V., Pikhtin N.A., Slipchenko S.O., Sokolova Z.N., Stankevich A.L., Khomylev M.A., Shamakhov V.V., Borschev K.S., Arsent'ev I.N., Tarasov I.S. *Semiconductors*, **41**, 984 (2007).
60. Markus A., Chen J. X., Paranthoen C., Fiore A., Platz C., Gauthier-Lafaye O. *Appl. Phys. Lett.*, **82**, 1818 (2003).
61. Djie H.S., Ooi B.S., Fang X.-M., Wu Y., Fastenau J.M., Liu W.K., Hopkinson M. *Opt. Lett.*, **32**, 44 (2007).
62. US patent 6,816,525 dated 09.11.2004.
63. Kovsh A., Krestnikov I., Livshits D., Mikhrin S., Weimert J., Zhukov A. *Opt. Lett.*, **32**, 793 (2007).
64. US patent application 11/295.943 of 07.12.2005.
65. US patent application 60/911,706 of 13.04.2007.
66. US patent application 11/737,946 of 20.04.2007.
67. *Optical Signal-to-Noise Ratio and the Q-factor in Fiber-Optic Communication Systems*. Maxim application note HFAN 09.0.2 (www.maxim-ic.com).
68. Matin M.A., Song K.C., Robinson B.J., Simmons J.G., Thompson D.A. *Microwave Opt. Tech. Lett.*, **12**, 310 (1998).

69. Garbuzov D., Maiorov M., Menna R., Komissarov A., Khalfin V., Kudryashov I., Lunev A., DiMarco L., Connolly J. *Proc. SPIE Int. Soc. Opt. Eng.*, **4651**, 92 (2002).
70. Henry C.H., Henry P.S., Lax M. *IEEE J. Lightwave Technol.*, **2**, 209 (1984).
71. Agrawal G.P. *Phys. Rev. A*, **37**, 2488 (1988).
72. Nguyen L.V.T. *Technology Organization (Australia) Research Report DSTO-RR-0244* (2002).
73. Su H., Lester L.F. *J. Phys. D*, **38**, 2112 (2005).
74. Ghosh S., Pradhan S., Bhattacharya P. *Appl. Phys. Lett.*, **81**, 3055 (2002).
75. Klotzkin D., Bhattacharya P. *IEEE J. Lightwave Technol.*, **17**, 1634 (1999).
76. Malic E., Ahn K.J., Bormann M.J.P., Hoevel Ph., Schoell E., Knorr A., Kuntz M., Bimberg D. *Appl. Phys. Lett.*, **89**, 101107 (2006).
77. Krakowski M., Resneau P., Calligaro M., Huiyun L., Hopkinson M. *IEEE 20th Int. Semicond. Las. Conf.* (Hawaii, USA, Sept. 17 – 21, 2006) p. 17.
78. Capua A., Rozenfeld L., Mikhelashvili V., Einstein G., Kuntz M., Laemlim M., Bimberg D. *Opt. Express*, **15**, 5388 (2007).
79. Schimpe R.Z. *Phys. B – Condensed Matter*, **52**, 289 (1983).
80. Gubenko A., Krestnikov I., Livshtis D., Mikhrin S., Kovsh A., West L., Bornholdt C., Grote N., Zhukov A. *Electron. Lett.*, **43**, 1430 (2007).